ACS APPLIED MATERIALS & INTERFACES

Research Article

www.acsami.org

Template-Particle Stabilized Bicontinuous Emulsion Yielding Controlled Assembly of Hierarchical High-Flux Filtration Membranes

Samuel C. Hess, A. Xavier Kohll, Renzo A. Raso, Christoph M. Schumacher, Robert N. Grass, and Wendelin J. Stark*

Institute for Chemical and Bioengineering, ETH Zürich Wolfgang-Pauli-Strasse 10 CH-8093 Zürich Switzerland

Supporting Information

ABSTRACT: A novel solvent-evaporation-based process that exploits template-particle stabilized bicontinuous emulsions for the formation of previously unreached membrane morphologies is reported in this article. Porous membranes have a wide range of applications spanning from water filtration, pharmaceutical purification, and battery separators to scaffolds for tissue engineering. Different situations require different membrane morphologies including various pore sizes and pore gradients. However, most of the previously reported membrane preparation procedures are restricted to specific morphologies and morphology alterations require an extensive optimization process. The tertiary system presented in this article, which consists of a poly(ether sulfone)/dimethylacetamide (PES/DMAc) solution, glycerol, and ZnO-nanoparticles, allows simple and exact tuning of pore diameters ranging from sub-20 nm, up to 100 nm. At the same time, the pore size gradient is controlled from 0 up to 840%/μm yielding extreme asymmetry. In addition to structural analysis, water flux rates of over 5600 L m^{-2} h^{-1} are measured for membranes retaining 45 nm silica beads.

KEYWORDS: *hierarchical membranes, template-particles, asymmetric structures, filtration, phase separation*

INTRODUCTION

Porous membranes enable drinking water purification,[1] biotechnological downstream processes,[2] battery separators,[3] reverse osmosis,[4] and food[5] separation processes. Depending on their specific application, different membrane morphologies are required. For the convenient separation of particles such as tiny parvoviruses from pharmaceutical goods, membranes thick and flexible enough to be mechanically stable while exhibiting appropriate pore sizes are desired. However, the assumption of symmetric pores predicts a linear decrease of flux with an increasing membrane thickness as set out by the law of Hagen Poiseuille[6] (eq 1)

$$V \approx \frac{d^2}{t} \tag{1}$$

where V is the volume flow, d the pore diameter, and t the membrane thickness. Consequently, efficient dead-end filtration membranes mostly exhibit asymmetric structures in order to minimize the thickness of the selective layer, which contains small flux-limiting pores. Today, many synthesis approaches aim to produce asymmetric high-flux membranes using methods including thermally induced phase inversion,[7] bicontinuous microemulsions,[8] and particle stabilized microemulsions,[9] block copolymers,[10−13] track etch,[14] supercritical gel drying,[15] and the nanoparticle template removal technique.[16] The currently most established method for producing porous membranes in a larger scale is the phase inversion,[17] a process where a polymer-rich casting solution is immersed in a nonsolvent bath. Casting solutions that lead to many well performing membranes can contain components including mixtures of polymers, additives, and solvents. However, the process of phase inversion is not yet fully understood, limiting the fast design and optimization of new and already existing membranes. The key-obstacle is the difficulty of controlling kinetics while the fast demixing process of the aforementioned substitutes as the casting solution enters the coagulation bath. Furthermore, this limiting step minimizes the free choice of polymers and additives as well as the range of options for their combination.

Here we report a novel filtration membrane fabrication procedure allowing the simple and exact shaping of porous polymer membranes with unexpected, previously unmaintained asymmetric properties. In addition to the method's simplicity and the large scale availability of all the ingredients it has great upscale-potential via roll-to-roll coating.[18] Furthermore, this method could be adapted to many other polymer/solvent-

Received: October 2, 2014
Accepted: December 16, 2014
Published: December 16, 2014

DOI: 10.1021/am506737n
ACS Appl. Mater. Interfaces 2015, 7, 611−617

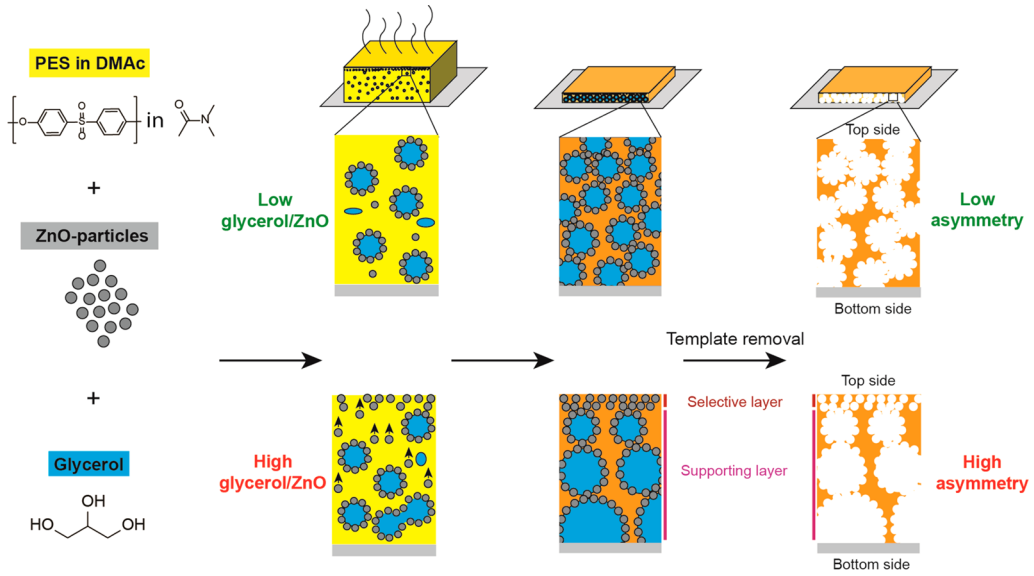

Figure 1. Asymmetric membrane production. From left to right: A PES solution in DMAc is mixed with soluble nanoparticles as pore templates and a second liquid (e.g., glycerol). Casting on a glass plate yields composite films. During solvent evaporation a thin top layer of nanoparticles was observed for high glycerol/ZnO ratios. After solvent evaporation and polymer coagulation the pore templating nanoparticles are dissolved with diluted HCl. We apply the terminologies "bottom side" for the membrane side facing the carrier (glass plate), and "top side" for the selective layer facing the air (i.e., where the solvent has evaporated). Within the selective layer which is located below the membrane's top side, the pores exhibit the narrowest diameter. The supporting layer follows below this selective top layer.

additive-nanoparticle emulsions than the PES/DMAc-glycerol-ZnO nanoparticle combination described here.

The stable membrane formation is enabled by physically well investigated phenomena, namely, spinodal decomposition of particle stabilized binary liquids[9,19] and the usage of template particles as such.[16] Membranes produced with varying ingredients concentrations and varying process parameters were analyzed on their morphology at different steps during membrane synthesis. This allowed deciphering most of the membrane formation mechanism, as well as the key parameters for guiding the pore size and pore size gradient. By only varying the concentration ratio of glycerol and ZnO nanoparticles, pore sizes form sub-20 nm up to 100 nm and various pore size gradients could be reproducibly created. A selection of membranes was finally tested on pure water flux rates as well as silica nanoparticle retention rates, and compared to commercially available high-end virus filters.

EXPERIMENTAL SECTION

Membrane Preparation. Poly(ether sulfone) (PES) (Veradec, A-201) 9 wt % was solved in dimethylacetamide (DMAc), than mixed with ZnO-nanoparticles (Zincox 10, IBUtec) and either glycerol (Sigma-Aldrich, ≥ 99.5%), triethylene glycol (TEG) (Sigma-Aldrich 99%) or polyethylene glycol (PEG) 200 (Acros). The particles were dispersed with an ultrasonic horn (Hielscher UP 400s, Germany) by sonicating for 1 min at 400 W. A spiral film applicator (Zehntner, ZAA2300, 50 μm spiral) was used for producing films of A4 size. After the films were dried in an oven at 100 °C for 5 min, the ZnO-nanoparticles and additives were extracted by incubating the film in a 1 M HCl bath for 5 min followed by incubation for 5 min in a water bath for removing the acid.

SEM Analysis. An FEI nova NanoSEM 450 was used at 3 kV and spot-size 2.5. The samples were coated with 3 nm of platinum (Leica EAA, SCD005). For analyzing cross sections, the membranes were broken after cooling them with liquid nitrogen. Pore size distribution: The surface-area of at least 150 pores per sample was measured manually by Photoshop analysis. Cross section gradient: Six equally distributed lines, parallel to the surfaces, were drawn along the cross section for each sample, at arbitrary location. The data points in Figure 3b correspond to the average pore-size along these lines.

Liquid Chromatography Mass Spectrometry (LC-MS) Analysis. All membrane samples were solved in DMAc (Sigma-Aldrich, ≥ 99.9, 1:10 wt %). The solvent consisted of 90 wt % tetrahydrofuran (Sigma-Aldrich, ≥ 99.9), 9.9 wt % methanol (FisherBio, LC/MS grade), and 0.1 wt % formic acid (FisherBio, LC/MS grade). We run 0.5 mL/min at 40 °C through a Zorbax column Eclipse XDB 4.6 × 150 mm using an Agilent 1100 Series LC device coupled with a MSD.

Nitrogen Adsorption/Desorption Measurements. The nitrogen adsorption/desorption measurements at 77 K were conducted using a Micrometrics TriStar II 3020 V1.03. The BJH Desorption Cumulative Pore Area was used for estimating the pore-size distribution. Prior to the measurements the samples were degassed at RT under a pressure of 10^{-4} mbar.

Pure Water Flux Measurements. All the measurements were conducted with an in-house built filtration device. A filtration area of 0.8 cm^2 and a constant pressure of 2 bar were used. To subtract any flux reducing effects occurring because of membrane compaction,[21] we conservatively measured the pure water flux (PWF) after 2 h on stream.

Nanobead Retention Test. The following nanobeads were used: sicastar-greenF (micromod), plain, 25 nm, at a concentration of 250 $\mu g\ mL^{-1}$. SPHERO Carboxyl Fluorescent particles (Spherotech), Nile Red, 45 nm at a concentration of 0.01 w/v %. Three milliliters per measurement were used. The fluorescence of the filtrate was measured using a plate reader (Tecan, infinite F200). For the sicastar-greenF beads 485/535 nm (excitation/emission) and the for the SPHERO Carboxyl Fluorescent particles in Nile Red frequencies of 540/620 nm were used.

Polymer Solution Viscosity Measurement. The viscosity of a 9 wt % PES solution (in DMAc) plus 100 wt % (respective to the PES) glycerol was measured on a ARES-G2 device. The measurement was conducted at 50 °C (in a forced convection oven) with parallel plates of 50 mm in diameter and a gap of several 0.1 mm. The shear rate ramp was 1−100 and 100−1 s^{-1}, 15 s each ramp.

RESULTS AND DISCUSSION

Membrane Synthesis and Pore-Size Variation. Casting solutions were prepared from mixing PES dissolved in DMAc,

DOI: 10.1021/am506737n
ACS Appl. Mater. Interfaces 2015, 7, 611−617

ZnO-nanoparticles with an average diameter of 20 nm and one polyfunctional alcohol (glycerol, TEG or PEG 200). After casting the membrane-film onto a glass plate and drying it via solvent evaporation, the soluble nanoparticles, as well as the additives, were removed using a weakly acidic bath (see Figure 1). All concentrations are given as a ratio, e.g. 70/30 50 wt %, meaning the wt. ratio of ZnO-nanoparticles to PES followed by the wt % of additive relative to the mass of PES.

We detected enormous alterations in the membrane morphology while varying the casting solution composition. Specifically, concentrations of glycerol and template ZnO nanoparticles were discovered to be the key parameters in exactly controlling the pore size and pore gradient along the membrane cross-section. To systematically investigate the influence of increasing glycerol concentration as an additive, we initially set a constant ZnO/PES ratio of 70/30 wt %. This composition allows reliable porous membrane preparation without a second liquid phase (i.e., no additive). We gradually increased the glycerol concentration up to 100 wt % (with respect to the polymer weight). Starting at a mean pore diameter of 19.5 nm for additive-free membranes, the pore-size increased with the additive content. Optical evaluation by SEM of at least 150 pores was used to measure the pore size distributions (see Supporting Information Figure S1 and S2). The average pore size as a function of the additive content is illustrated in Figure 2. The reason for coupling glycerol content

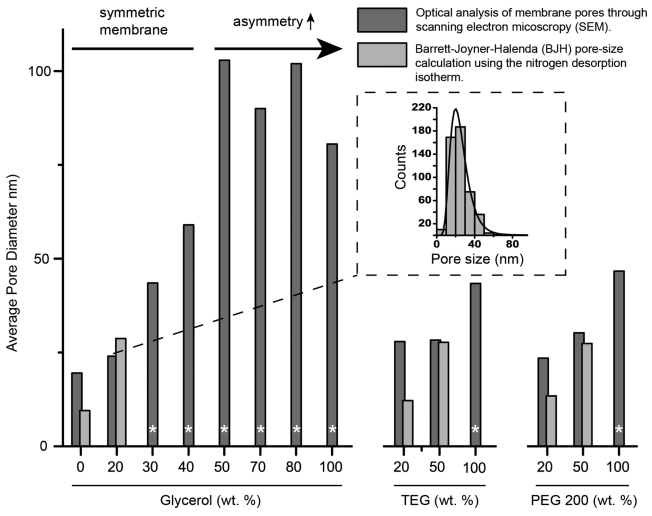

Figure 2. Control on pore size through additive concentration variation. The average pore size of membranes produced with of 70/30 (wt % ZnO/wt % PES) and varying concentrations of second-phase liquids (e.g., glycerol, TEG, and PEG 200) were obtained by SEM image analysis and nitrogen desorption analysis. The pore sizes reflect an average diameter of at least 150 pores within the selective layer. The asterisk (*) indicates that nitrogen adsorption/desorption was not applicable as the specific surface area of these samples was insufficient.

and pore size increase might initially seem surprising as well-established phase inversion usually applies glycerol as a coagulant for pore size minimization.[22] However, during synthesis of our membranes, glycerol could be considered as a pore forming spacer, which, similarly to the template nanoparticles is washed out of the polymeric matrix by acid bath incubation. In order to investigate the phenomenon of pore size increase in greater detail, we analyzed membranes produced with 20 and 50 wt % glycerol by SEM at two points during the preparation, that is, before and after particles were etched out (Figure 3a). Increasing the glycerol concentration

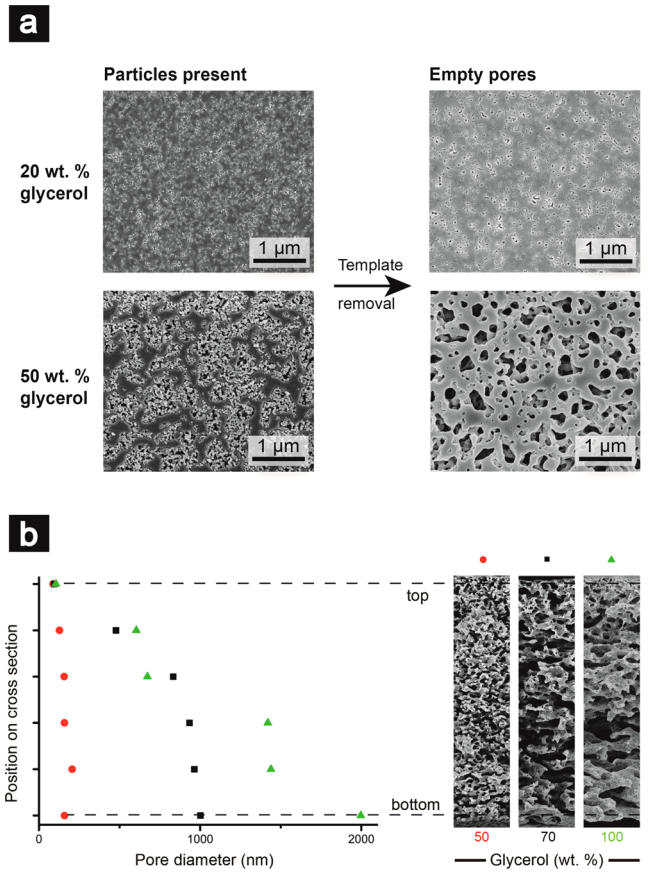

Figure 3. Increase of pore size and gradient along the cross section with increasing amount of glycerol. (a) PES membranes (70/30) prepared with 20 or 50 wt % of glycerol. The left side pictures display samples before the acid wash and nanoparticle removal, that is, the ZnO-particles are still present. The right side illustrates the empty pores within the membranes. All images were taken with the same magnification. (b) Illustration of the pore diameter as a function of the position on the cross section. The analyzed membranes (70/30) were prepared from mixtures containing 50, 70, or 100 wt % glycerol.

from 20 to 50 wt % clearly increased the agglomeration of nanoparticles in this highly packed system of ZnO/PES (70/30; high solid loading). Interestingly, the effect was broadly applicable, as substituting glycerol by TEG or PEG 200 afforded similarly robust behavior at comparable additive concentrations (see Figure 2, right). To independently confirm the SEM pore-size analysis, the pore-size distributions were also calculated with the Barrett–Jones–Halenda (BJH) method using nitrogen desorption isotherms as latter is favored for mesoporous structures.[23] Since this method is only suitable for measuring pores in the lower nanometer range, a limited number of samples could be meaningfully analyzed. Adding more glycerol than polymer (over 100 wt %) to a 70/30 (ZnO/PES) ratio mixture lead to membranes with decreased overall stability and homogeneity.

Gradient Formation within Highly-Packed Systems. Interestingly, increasing the glycerol content beyond 50 wt % did not enlarge the pore-size at the top side any more (Figure 2, Supporting Information Figure S1). To further decipher the complex morphological changes during preparation, the top

DOI: 10.1021/am506737n
ACS Appl. Mater. Interfaces 2015, 7, 611–617

side analysis was supplemented by an investigation of a series of bottom sides and cross sections of membranes (70/30). A glycerol content of up to 50 wt % during preparation lead to a symmetrical pore size increase on both the top-and bottom side. At 50 wt % glycerol, the symmetric cross-section displayed a surface pore size close to 100 nm at both sides. Significant deviations, however, occurred on the top and bottom when the glycerol concentration was further increased up to 100 wt %. While the top layer was not affected by further increasing the glycerol concentration, the average pore size on the bottom side grew from 100 nm to 1 and 2 μm for glycerol concentrations of 70 or 100 wt %, (Figure 3b). The volume ratio of PES to glycerol decreased from 65/35 to 57/43 and 48/52. For the quantification of the membrane's asymmetry, we measured the average pore size along the membranes' cross sections. These pore size profiles were plotted as a function of their position in the membrane's cross section (Figure 3b). To better compare membrane gradients we introduced a measure, which describes the increase of pore size in %/μm along the cross section assuming a linear increase. Therefore, the variation in size of the top and bottom pores of the membranes with a thickness between 8 and 11 μm were taken into account. Membranes produced with 70 wt % of glycerol exhibited a gradient of 124%/μm, which grew up to 208%/μm for a glycerol value of 100 wt %. The increase of the gradient lead to a reduction of the depth selective layer size from 100% to about 5% of the total membrane thickness (Supporting Information Figure S11).

Initially, the ratio of DMAc to PES/glycerol within the used casting solution allowed a homogeneous mixture, which after adding the ZnO particles formed a stable dispersion. During progressing solvent evaporation the PES/DMAc−glycerol−ZnO system reached a point, where the immiscible PES and glycerol underwent spinodal demixing. Jaiswal et al.[24] modeled the growth of an initial gradient caused by solvent evaporation on the surface of a thin layer over different periods of time, a phenomena termed surface-directed spinodal decomposition. Because of structural analysis, we believe that the gradient formation within the investigated bicontinuous liquids during solvent evaporation could arise from surface-directed spinodal decomposition. We experimentally confirmed Jaswal et al.'s prediction of increasing asymmetry for prolonged demixing times (samples with 70/30 100%). The phase separation time for this mixture can be controlled by the heating rate (i.e., rate of solvent evaporation). Lower temperatures (e.g., 50 °C) lead to increased spinodal decomposition affording membranes with bigger internal cavities. As an independent confirmation, the effect significantly decreased when the membrane preparation experiments were repeated at temperatures of 100 °C or even 130 °C (rapid solvent evaporation, see Supporting Information Figures S5, S6, and S7). We additionally tested the robustness of gradient formation by drying membranes "up-side-down" and, thereby, reversing the gravitational impact on the system. Even these changes did not inhibit the gradient formation as illustrated in Supporting Information Figure S8.

Effect of Particle Loadings on the Formation of Droplet-like, Asymmetric and Symmetric Membranes. The morphological variations described until now all involved a constantly high ZnO to PES ratio of 70/30. However, regardless the PES to glycerol ratio and film drying time, template particle concentration was identified as an additional key parameter influencing the system's pore-size. Tuning the particle concentration yielded even more extreme membrane internal gradients and more defined selective layers. Within that system, the nanoparticles seem to be sequestrating at the interfacial surface of the two immiscible liquids, similar to bicontinuous interfacially jammed emulsion gels, also called "bijels".[19] As illustrated in Figure 3b, with increasing amounts of glycerol and a fixed ratio of PES/ZnO the pore size of the percolating system is growing, a typical behavior of bicontinuous systems with particle stabilized interfaces.[9,19,25]

We therefore expect the membrane cavity size within the supportive layer to increase if the ratio of ZnO-particles to glycerol is lowered. While keeping the glycerol content at 50 wt % (with respect to polymer weight), we systematically lowered the ZnO-particle to PES ratio from 70/30 to 60/40, 50/50 and 30/70 (Figure 4). For decreasing particle concentration,

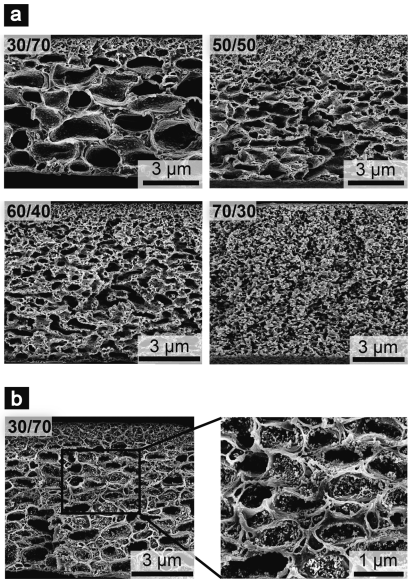

Figure 4. Asymmetry as function of template particle content. (a) All membranes were produced with 50 wt % of glycerol (with respect to the PES content)). Four ratios of ZnO/PES were used: 30/70, 50/50, 60/40, and 70/30 (wt %/wt %). (b) A 30/70 membrane before dissolving the ZnO-nanoparticles with acid.

asymmetric structures with increasing cavity size evolved. When reducing the ratio from 50/50 to 30/70 a transition between bicontinuous, percolating structures and droplet-like structures occurred (Figure 4a, 30/70).

The formation of droplet-like emulsions and subsequent transformation into spherically shaped cavities was confirmed through detailed analysis of the 30/70 membrane's cross section before acid treatment (i.e., still containing the ZnO nanoparticles, Figure 4b). The magnified area (Figure 4b, right side) highlights particles still located on the polymeric surface, which is the former interface between glycerol and polymer liquid domains. Additionally imprints of the same size as the ZnO template particles were confirmed on the polymeric pore surface of membranes after removing the particles (Supporting Information Figure S10).

Importantly, compared to high ZnO concentrations, the membrane's top-layer exhibited no bicontinuous or characteristic spinodal patterns and single or small agglomerates of nanoparticles dominated its structure at the lower ZnO/PES ratios (Supporting Information Figure S9). This behavior resulted in a decrease of the top layer pore size and pore size distribution, a contrast to membranes containing the same

DOI: 10.1021/am506737n
ACS Appl. Mater. Interfaces 2015, 7, 611−617

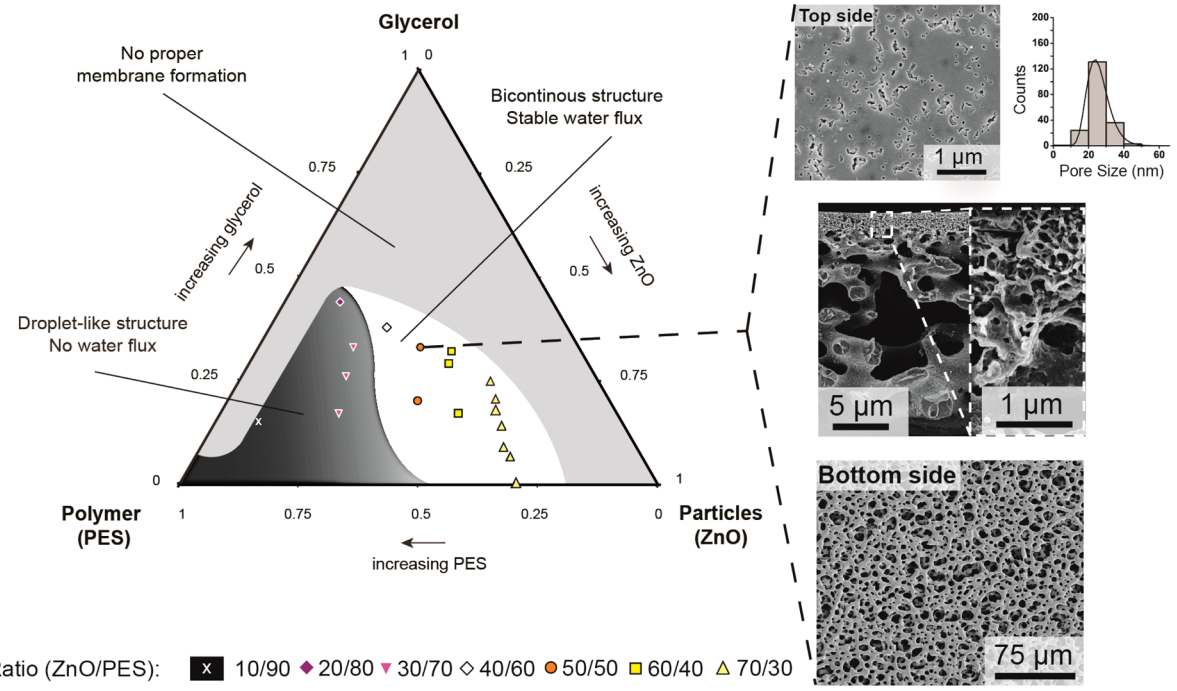

Figure 5. Three-Component Diagram. Left side: Diagram illustrating the relation between the casting solution composition and the resulting membrane's properties. Compositions within the gray area lead to no stable membrane, the ones in the white area result in bicontinuous structures with stable flux. The compositions within the black area lead to droplet-like structures and membranes without water flux. The ratio (wt % ZnO/wt % PES) of different membrane series is presented in the legend. Right side: images of a membrane made of 50/50 (ZnO/PES) and 100 wt % of glycerol, including top view, side view plus magnification of the thin selective layer (top) and bottom view.

amount of glycerol, but higher particle loadings. Routh et al.[20] have modeled a phenomena called skinning, which describes the diffusion of spherically shaped particles to the top layer of thin films forming a skin layer during solvent evaporation (illustrated in Figure 1). They stated that if the particle's diffusion rate is much larger than the time for evaporation (Peclet number much greater than one)

$$H\dot{E}/D_0 \gg 1 \qquad (2)$$

where H is the thickness, $\dot{E}$ the surface reduction rate, and D_0 the diffusion coefficient, a fraction of the initially well dispersed particles will form a skin on top of thin films (eq 2).[20] As the Peclet number in our system is exceeding one, the requirements for skinning seem to be fulfilled (see Supporting Information Skinning of Particles).

Designing Ultra-High Membrane Gradients. With the aim of producing a stable, mesoporous membrane with a maximum gradient and narrow pore size distribution within a thin selective layer, we selected an intermediate mixture of ZnO/PES/glycerol of 1/1/1 by weight (50/50, 100% glycerol). Concluding from SEM analysis (Figure 5, right side), the top layer exhibited pores mostly caused by single template particles or agglomerations of a few particles resulting in an average-pore size of 25 nm (see pore-size distribution Figure 5). Pores on the bottom side exhibited an average diameter of 4.2 μm, indicating a pore size increase over a 20 μm thick cross section of more than 160 times, resulting in a gradient-value of 840%/μm, again assuming a linear increase in pore size. This image analysis confirmed that these mixtures lead to a casting solution favoring a polymer skin formation containing mostly single particles, while maintaining a high pore gradient within the rest of the membrane.

We summarized the key properties of different membranes in a three-dimensional diagram (Figure 5) for various initial liquid compositions. At low glycerol and ZnO concentration, droplet-like structures afford polymer films with no water flux (Figure 5, black area). If the ratio of glycerol to ZnO nanoparticles exceeds a certain threshold uncontrolled spinodal demixing takes place and the resulting inhomogeneity leads to instable membranes. In case a too low polymer to ZnO/glycerol ratio is used, no stable membranes could be formed either (Figure 5, gray area). Stable, bicontinuous structures yielding membranes with reliable, technically attractive water flux occur for the remaining intermediate concentrations (see Figure 5, white area).

In order to detect potentially remaining polyfunctional alcohols in the final membranes, LC-MS was conducted from the membrane samples dissolved in DMAc. Membranes that were produced with high concentrations of additives (100 wt % of glycerol, 150 wt % of TEG, 150 wt % of PEG 200) finally contained TEG of around 0.05 wt % and a PEG 200 concentration below 0.05 wt %. Because of the unfavorable detection limit of glycerol within the PES/DMAc no valuable answer could be gained for this additive. Considering glycerol's small molecule size and its similar properties compared to the above used ethylene glycols, it can be assumed that the glycerol residuals range in a similar or lower order of magnitude to those of membranes containing TEG or PEG 200.

Filtration and Bead Retention Tests. Finally, to test the accuracy and performance of the ultrafiltration membranes obtained, we conducted PWF measurements and bead retention tests with fluorescent silica of 25 or 45 nm in diameter. All the tested membranes consisted of PES and therefore interact similarly with the test particles, allowing the comparison of retention results. Membranes containing 70/30

DOI: 10.1021/am506737n
ACS Appl. Mater. Interfaces 2015, 7, 611−617

(ZnO/PES) and various additive concentrations were compared to commercially available high-end virus filtration membranes (Sartorius, Virosart CPV and Millipore, Viresolve pro), which we assume are representing the state of the art in phase inversion (Table 1). The PWF rates for membranes

Table 1. Comparison to Commercial Phase Inversion Derived Membranes[a]

membrane	retention 25 nm silica beads [%]	retention 45 nm silica beads [%]	pure water flux [L m^{-2} h^{-1}] at 2 bar after 2 h
no additive	99.93 ± 0.00	[c]	49 ± 8
20% glycerol	99 ± 0	97 ± 4	140 ± 30
30% glycerol	91 ± 8	94 ± 3	960 ± 90
50% glycerol	28 ± 8	80 ± 5	2800 ± 170
70% glycerol	[c]	97 ± 1	5400 ± 150
20% PEG 200	99.97 ± 0.04	[c]	90 ± 5
50% PEG 200	99.91 ± 0.05	[c]	740 ± 40
100% PEG 200	33 ± 8	[c]	4800 ± 300
Sartorius Virosart CPV Minisart	99.9[b]	[c]	108[b]
Millipore Viresolve Pro	82[b]	[c]	348[b]

[a]Membranes containing 70/30 and varying amounts of glycerol (0, 20, 30, 50, 70 wt % with respect to PES wt %) or PEG 200 (20, 50, 100 wt % with respect to PES wt %) were tested for retention of 25 or 45 nm silica particles. Two commercial membranes were tested as well. Additionally the pure water flux was measured for comparison. For our own membranes: $N = 3$, errors are calculated by the standard error of the mean. [b]Only measured once. [c]Not measured.

produced with TEG can be found in Supporting Information Table S2. For better reliability in order to take the potential membrane compaction (flux reductions in PES membranes up to 60%)[21] into full account, the PWF was measured after 2 h on stream. Sartorius Virosart CPV retaining 99.9% of 25 nm silica beads exhibited a PWF of 104 L/m^2/h at 2 bar, and the Millipore Viresolve pro retaining 82% of 25 nm beads performed a PWF of 348 L/m^2/h at 2 bar. These measurements seem to illustrate the trade-off between PWF and the retention capacity. Surprisingly 70/30 (ZnO/PES) manufactured membranes using 50 wt % of PEG 200 retained 99.91% of 25 nm silica beads still allowing a PWF of 740 L/m^2/h at 2 bar, which is over seven times more than the Virosart CPV filter with similar bead retention.

In general, the PWF increased and the bead retention for 25 nm particles decreased with increasing additive content as expected. To illustrate the impact of asymmetric membrane design (Figure 6), we calculated the theoretical flux while assuming symmetric pores of equal size throughout a cross section and used the law of Hagen–Poiseuille[6] (eq 1). For 70/30 (ZnO/glycerol) membranes containing up to 50 wt % of glycerol (mostly symmetric), the measured flux was slightly higher than the calculated flux.

Even though no significant gradient occurs at those additive concentrations yet, glycerol may have promoted the pore-system's connectivity. Increasing the glycerol concentration from 50 to 70 wt % nearly doubled the pure water flux from 2800 to 5600 L/m^2/h at 2 bar, regardless of the average pore size of the top layer even slightly dropped. The 45 nm bead retention increased from 80 to 97% for this increase of glycerol (see Table 1).

CONCLUSIONS

In summary, our novel membrane fabrication procedure successfully combines bicontinuous particle stabilized emulsions with the template removal technique, enabling a simple and effective control of membrane morphologies. Specifically, we tuned the thickness of the membrane's selective layer from a couple of 100 nm to tens of micrometers and varied the pores size gradient along the cross section form symmetric to highly asymmetric channels. Furthermore, the template ZnO nanoparticles used in this study allowed selective pore formation from below 20 nm up to 100 nm. Within further studies, we plan to determine the membrane's selectivity, meaning the ratio of filtrate recovery and rejected particles. Besides the field of filtration, this novel technique potentially opens up new opportunities in the area of tissue engineering,[26,27] tunable particle stabilized bicontinuous microemulsions[8] and solar cell research.[28,29] For all of these fields tunable porous structures in the nano-or micrometer range without (particles removed) or in combination with nanoparticles have great potential.

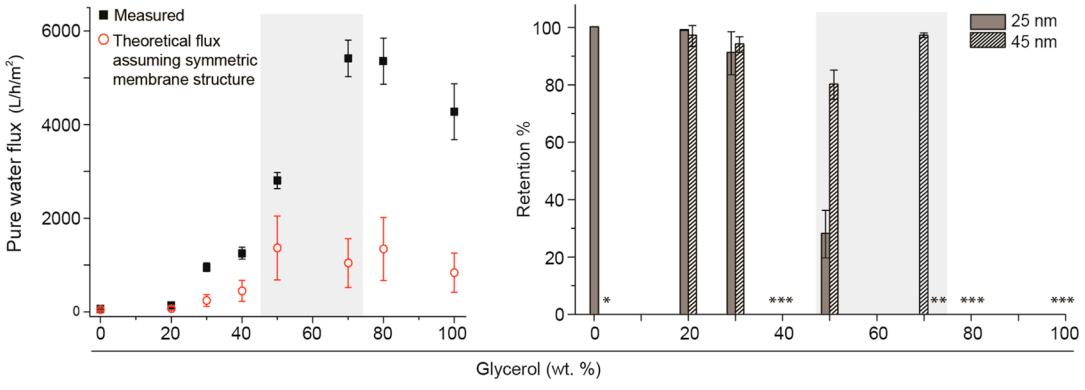

Figure 6. Bead retention and flux rates. Left sided graph: Measured pure water flux and calculated flux assuming symmetric membrane structure as a function of a membrane's glycerol content. Right graph: 25 and 45 nm silica nanobead retention analysis. The gray shaded blocks in both graphs highlight the increase in flux while maintaining good 45 nm bead retention as a consequence of the increasing asymmetry within the membrane. * 45 nm bead-retention not measured as the 25 nm beads are retained, ** 25 nm bead-retention not measured as they already passed the membranes containing 50 wt % of glycerol. *** not tested.

DOI: 10.1021/am506737n
ACS Appl. Mater. Interfaces 2015, 7, 611–617

■ ASSOCIATED CONTENT

Supporting Information

Further pore-size distribution analysis plus SEM images of membranes dried under different conditions. This material is available free of charge via the Internet at http://pubs.acs.org.

■ AUTHOR INFORMATION

Corresponding Author

*E-mail: wendelin.stark@chem.ethz.ch.

Author Contributions

S.H., C.S., R.G., and W.J.S elaborated the concept, S.H. led the project and performed all experimental work with support of X.K., with the exception of HPLC analysis, which was performed by R.R., and the BET measurements, which were conducted by Tobias Keller, PhD candidate in the laboratory of Prof. Dr. Javier Pérez-Ramírez. S.H. prepared all figures and the manuscript was written by S.H., R.G., and W.J.S.

Notes

The authors declare the following competing financial interest(s): W.J.S. declares financial interest in form of a patent application. S.H., X.K., R.R., and R.G. declare no competing financial interest.

■ ACKNOWLEDGMENTS

Financial support by ETH Zurich and the Swiss National Science Foundation (No. 406440-131268) is kindly acknowledged. The authors gratefully acknowledge the BET measurements conducted by Tobias Keller, PhD candidate in the laboratory of Prof. Dr. Javier Pérez-Ramírez, ETH-Zürich. Furthermore, we would like to thank Thomas Schweizer from the Institute for Polymers at the ETH-Zürich for the conducted viscosity measurements.

■ REFERENCES

(1) Shannon, M. A.; Bohn, P. W.; Elimelech, M.; Georgiadis, J. G.; Marinas, B. J.; Mayes, A. M. Science and Technology for Water Purification in the Coming Decades. *Nature* **2008**, *452*, 301−310.

(2) Rathore, A. S.; Shirke, A. Recent Developments in Membrane-Based Separations in Biotechnology Processes: Review. *Prep. Biochem. Biotechnol.* **2011**, *41*, 398−421.

(3) Liu, H. Y.; Liu, L. L.; Yang, C. L.; Li, Z. H.; Xiao, Q. Z.; Lei, G. T.; Ding, Y. H. A Hard-Template Process to Prepare Three-Dimensionally Macroporous Polymer Electrolyte for Lithium-Ion Batteries. *Electrochim. Acta* **2014**, *121*, 328−336.

(4) Kosutic, K.; Kastelan-Kunst, L.; Kunst, B. Porosity of Some Commercial Reverse Osmosis and Nanofiltration Polyamide Thin-Film Composite Membranes. *J. Membr. Sci.* **2000**, *168*, 101−108.

(5) Makardij, A.; Chen, X. D.; Farid, M. M. Microfiltration and Ultrafiltration of Milk: Some Aspects of Fouling and Cleaning. *Food Bioprod. Process.* **1999**, *77*, 107−113.

(6) Pfitzner, J. Poiseuille and His Law. *Anaesthesia* **1976**, *31*, 273−275.

(7) Matsuyama, H.; Yuasa, M.; Kitamura, Y.; Teramoto, M.; Lloyd, D. R. Structure Control of Anisotropic and Asymmetric Polypropylene Membrane Prepared by Thermally Induced Phase Separation. *J. Membr. Sci.* **2000**, *179*, 91−100.

(8) Jones, B. H.; Lodge, T. P. Nanocasting Nanoporous Inorganic and Organic Materials from Polymeric Bicontinuous Microemulsion Templates. *Polym. J. (Tokyo, Jpn.)* **2012**, *44*, 131−146.

(9) Herzig, E. M.; White, K. A.; Schofield, A. B.; Poon, W. C. K.; Clegg, P. S. Bicontinuous Emulsions Stabilized Solely by Colloidal Particles. *Nat. Mater.* **2007**, *6*, 966−971.

(10) Yang, S. Y.; Park, J.; Yoon, J.; Ree, M.; Jang, S. K.; Kim, J. K. Virus Filtration Membranes Prepared from Nanoporous Block Copolymers with Good Dimensional Stability under High Pressures and Excellent Solvent Resistance. *Adv. Funct. Mater.* **2008**, *18*, 1371−1377.

(11) Peinemann, K. V.; Abetz, V.; Simon, P. F. W. Asymmetric Superstructure Formed in a Block Copolymer via Phase Separation. *Nat. Mater.* **2007**, *6*, 992−996.

(12) Madhavan, P.; Peinemann, K. V.; Nunes, S. P. Complexation-Tailored Morphology of Asymmetric Block Copolymer Membranes. *ACS Appl. Mater. Interfaces* **2013**, *5*, 7152−7159.

(13) Schacher, F.; Rudolph, T.; Wieberger, F.; Ulbricht, M.; Muller, A. H. E. Double Stimuli-Responsive Ultrafiltration Membranes from Polystyrene-*block*-Poly(*N*,*N*-Dimethylaminoethyl Methacrylate) Di-block Copolymers. *ACS Appl. Mater. Interfaces* **2009**, *1*, 1492−1503.

(14) Apel, P. Track Etching Technique in Membrane Technology. *Radiat. Meas.* **2001**, *34*, 559−566.

(15) Cardea, S.; Gugliuzza, A.; Sessa, M.; Aceto, M. C.; Drioli, E.; Reverchon, E. Supercritical Gel Drying: A Powerful Tool for Tailoring Symmetric Porous PVDF-HFP Membranes. *ACS Appl. Mater. Interfaces* **2009**, *1*, 171−180.

(16) Kellenberger, C. R.; Luechinger, N. A.; Lamprou, A.; Rossier, M.; Grass, R. N.; Stark, W. J. Soluble Nanoparticles as Removable Pore Templates for the Preparation of Polymer Ultrafiltration Membranes. *J. Membr. Sci.* **2012**, *387*, 76−82.

(17) Solomon, B. R.; Hyder, M. N.; Varanasi, K. K. Separating Oil−Water Nanoemulsions using Flux-Enhanced Hierarchical Membranes. *Sci. Rep* **2014**, *4*, 5504.

(18) Kellenberger, C. R.; Hess, S. C.; Schumacher, C. M.; Loepfe, M.; Nussbaumer, J. E.; Grass, R. N.; Stark, W. J. Roll-to-Roll Preparation of Mesoporous Membranes by Nanoparticle Template Removal. *Ind. Eng. Chem. Res.* **2014**, *53*, 9214−9220.

(19) Cates, M. E.; Clegg, P. S. Bijels: A New Class of Soft Materials. *Soft Matter* **2008**, *4*, 2132−2138.

(20) Routh, A. F. Drying of Thin Colloidal Films. *Rep. Prog. Phys.* **2013**, *76*, 046603.

(21) Bohonak, D. M.; Zydney, A. L. Compaction and Permeability Effects With Virus Filtration Membranes. *J. Membr. Sci.* **2005**, *254*, 71−79.

(22) Holda, A. K.; Vankelecom, I. J. Integrally Skinned PSf-Based SRNF-Membranes Prepared via Phase Inversion-Part A: Influence of High Molecular Weight Additives. *J. Membr. Sci.* **2014**, *450*, 512−521.

(23) Thommes, M.; Smarsly, B.; Groenewolt, M.; Ravikovitch, P. I.; Neimark, A. V. Adsorption Hysteresis of Nitrogen and Argon in Pore Networks and Characterization of Novel Micro- and Mesoporous Silicas. *Langmuir* **2006**, *22*, 756−764.

(24) Jaiswal, P. K.; Binder, K.; Puri, S. Phase Separation of Binary Mixtures in Thin Films: Effects of an Initial Concentration Gradient Across the Film. *Phys. Rev. E* **2012**, *85*, No. 041602.

(25) Herzig, E. M.; White, K. A.; Schofield, A. B.; Poon, W. C. K.; Cates, M. E.; Clegg, P. S. The Bijel: A Bicontinuous Interfacially Jammed Emulsion Gel. *NSTI Nanotech 2008, Nanotechnol. Conf. Trade Show, Tech. Proc.* **2008**, 657−660.

(26) Madihally, S. V.; Matthew, H. W. T. Porous Chitosan Scaffolds for Tissue Engineering. *Biomaterials* **1999**, *20*, 1133−1142.

(27) Park, S. H.; Song, I. Y.; Lim, J.; Kwon, Y. S.; Choi, J.; Song, S.; Lee, J. R.; Park, T. A Novel Quasi-Solid State Dye-Sensitized Solar Cell Fabricated Using a Multifunctional Network Polymer Membrane Electrolyte. *Energy Environ. Sci.* **2013**, *6*, 1559−1564.

(28) Zhou, E.; Cong, J. Z.; Hashimoto, K.; Tajima, K. Control of Miscibility and Aggregation Via the Material Design and Coating Process for High-Performance Polymer Blend Solar Cells. *Adv. Mater.* **2013**, *25*, 6991−6996.

(29) Ahn, S. H.; Kim, D. J.; Chi, W. S.; Kim, J. H. Hierarchical Double-Shell Nanostructures of TiO_2 Nanosheets on SnO_2 Hollow Spheres for High-Efficiency, Solid-State, Dye-Sensitized Solar Cells. *Adv. Funct. Mater.* **2014**, *24*, 5037−5044.

DOI: 10.1021/am506737n
ACS Appl. Mater. Interfaces 2015, 7, 611−617